

## Two distinct non-Arrhenius behaviors of hydrogen diffusivities in fcc aluminum, silver, and copper determined by *ab initio* path integral simulations

Hajime Kimizuka<sup>1,\*</sup> and Motoyuki Shiga<sup>2</sup>

<sup>1</sup>*Department of Materials Design Innovation Engineering, Nagoya University, Aichi 464-8603, Japan*

<sup>2</sup>*Center for Computational Science and E-Systems, Japan Atomic Energy Agency, Chiba 277-0871, Japan*



(Received 23 March 2021; revised 27 May 2021; accepted 15 June 2021; published 25 June 2021)

Nuclear quantum effects (NQE) are highly important for understanding a host of kinetic processes that occur with the participation of H (e.g., H adsorption, diffusion, permeation, and trapping in materials). In this paper, *ab initio* path integral molecular dynamics simulations were used to investigate NQEs on the lattice diffusion of H in common face-centered cubic (fcc) metals such as Al, Ag, and Cu over a wide temperature range of 75–1200 K (75–900 K for Al). We determined that the dependence of H diffusivities on temperature in Ag and Cu has a “reversed-S” shape on Arrhenius plots, as confirmed for fcc Pd in our recent study [H. Kimizuka *et al.*, *Phys. Rev. B* **100**, 024104 (2019)]. This result illustrates that the phenomenon is common in many fcc metals in which H atoms prefer to occupy octahedral sites. On the other hand, in the case of Al, in which H atoms prefer to occupy tetrahedral sites, the dependence of H diffusivities on temperature exhibits a familiar “C” shape. Such counterintuitive behavior is ascribed to differences in the dependence on temperature of the activation barriers for H migration between both types of fcc metals; this is due to the NQEs involving a competition between deceleration of H migration, which becomes effective at high temperatures because of zero-point vibrations, and acceleration of H migration, which becomes effective at low temperatures because of quantum tunneling. The dominance of the two mechanisms is determined by the coupling of the NQEs and the site preference of H depending on the metal. This finding has important implications for the interpretation of kinetic processes involving the crossover from classical to quantum behavior of H atoms jumping between different types of interstitial sites.

DOI: [10.1103/PhysRevMaterials.5.065406](https://doi.org/10.1103/PhysRevMaterials.5.065406)

### I. INTRODUCTION

Diffusion of interstitial H atoms in solids is a basic kinetic process that governs various phenomena related to the utilization of H as an energy resource. It is relevant to numerous applications such as microelectronics (use of H in fuel cells), new energy materials (production and storage of H), reactor safety (H-induced embrittlement), and sensors [1–5]. Because of its scientific and technological importance, the diffusion of H isotopes in body-centered cubic (bcc) and face-centered cubic (fcc) metals has been extensively investigated (for reviews, see Refs. [1,6,7]). Notably, with decreasing temperature, H diffusivity ( $D$ ) as a function of inverse temperature has long been known to deviate from the linear Arrhenius relation. More specifically, for bcc metals, the Arrhenius plots of  $D$  of H often show conventional “C”-shaped curves that, at low temperatures, deviate “upward” from the classical relation [1,6–13], whereas for some fcc metals [1,14–21], curves of different shapes that deviate “downward” are observed at intermediate temperatures. Although such different non-Arrhenius behaviors may arise from a certain coexistence of different mechanisms of quantum diffusion, a consensus regarding the physical mechanisms is still lacking.

Generally, the nuclear quantum effects (NQEs) [22,23] of lightweight H atoms, comprising zero-point motion, discrete vibrational levels, and tunneling, are essential for identifying the inherent nature and exact kinetics of H diffusion. Our previous computational studies [24,25] have demonstrated that the  $D$  of H isotopes in fcc Pd actually exhibits a “reversed-S”-shaped dependence on temperature, indicating the significance and underlying role of NQEs in a manner consistent with experimental measurements. Because the NQEs are supposed to behave nonlinearly with respect to inverse temperature and be more pronounced at low temperatures, establishing a numerical framework that properly accounts for NQEs is necessary for characterizing in detail the nature of H diffusion. This is also due to severe technical difficulties involved in measuring  $D$  accurately over a wide temperature range, which are attributable to the low solubility of H and the high sensitivity to defect-trapping effects in various metals.

In this paper, we present a general picture of the diffusion kinetics of H in common fcc metals, including Al, Ag, and Cu, to inductively characterize the dominant factors that lead to the C-shaped and reversed-S-shaped behaviors of  $D$  values in their Arrhenius plots. For this purpose, we provide theoretical estimates of  $D$  with NQEs over a wide temperature range of 75–900 K for Al and 75–1200 K for Ag and Cu based on *ab initio* path integral molecular dynamics (PIMD) simulations, which can consistently and coherently describe the onset of quantum tunneling at low temperature and transitions to the

\*kimizuka@nagoya-u.jp

classical system at high temperature. Although Al and Al alloys have been widely used in the industry as important structural materials, the injected H can significantly influence the microstructure and mechanical properties of the metal and limit the lifetime of the structural components [26]. Ag and Ag alloys are candidates for tritium permeation barrier materials in fusion reactors because of their low permeability for H isotopes, including tritium [27]. Although Cu and Cu alloys are prime candidates for high heat-flux applications in fusion energy systems [28], they are susceptible to H embrittlement, as in the case of Al and Al alloys. As the basic parameter that determines the kinetics of H-related processes in metal–H systems, the ideal H diffusivities obtained in this paper are highly important.

## II. METHODS

### A. DFT calculations

Density functional theory (DFT) calculations were performed using the Vienna *ab initio* Simulation Package (VASP) [29] with the projector-augmented wave (PAW) method [30,31]. The valence electron configurations considered in this study included  $1s^1$  for H,  $3s^23p^1$  for Al,  $4d^{10}5s^1$  for Ag, and  $3d^{10}4s^1$  for Cu. The exchange-correlation functional was described within the Perdew, Burke, and Ernzerhof (PBE) generalized gradient approximation [32]. We considered an  $M_{32}H_1$  ( $M = \text{Al, Ag, or Cu}$ ) supercell with dimensions of  $2a \times 2a \times 2a$  (where  $a$  is the lattice constant of the fcc unit cell) under periodic boundary conditions, in which one H atom was initially placed at one of the octahedral (O) or tetrahedral (T) interstitial sites in the fcc structure. Calculations were performed with a plane-wave energy cutoff ( $E_{\text{cut}}$ ) of 250–300 eV using a  $6 \times 6 \times 6$  Monkhorst–Pack  $k$ -point mesh [33] for integration over the Brillouin zone. The cell parameters and atomic positions were relaxed within the classical DFT regime (i.e., without NQEs) using the Methfessel–Paxton smearing method [34] at a width of 0.2 eV, until the residual forces acting on each atom were less than 10 meV/Å. We used the nudged elastic band method [35] with nine intermediate images and a constant cell shape to obtain the minimum energy paths (MEPs) and saddle-point (S) sites for H migration between different sites. Calculations with an  $E_{\text{cut}}$  of 400 eV and a  $16 \times 16 \times 16$   $k$ -point mesh provided similar values, with a maximum error of 16 meV (see Supplemental Material [36]).

To test the system size dependence of the results, additional calculations were performed using an  $M_{108}H_1$  supercell with dimensions of  $3a \times 3a \times 3a$ . The results showed that, whereas the energies almost converged with respect to cell size, the activation barriers for H migration increased by 8, 34, and 37 meV for Al, Ag, and Cu, respectively, compared with those obtained using the  $M_{32}H_1$  supercell (see Supplemental Material [36]). This raised a concern that such an underestimation of the H-migration barriers for the small supercell may lead to overestimation of the H diffusivities. In this paper, to obtain accurate results with NQEs in a computationally efficient manner, we used the  $M_{108}H_1$  supercell (with an  $E_{\text{cut}}$  of 250–300 eV and an  $8 \times 8 \times 8$   $k$ -point mesh) to determine the classical MEPs without NQEs, whereas the MEPs

obtained using the  $M_{32}H_1$  supercell were used as centroid intrinsic reaction coordinates along which the NQEs on the H-diffusion process were evaluated via *ab initio* PIMD calculations [37,38]. Such an approximation is typically acceptable when the local shapes of the MEPs obtained from the two supercells are supposed to be compatible with each other. Another test using an  $M_{256}H_1$  supercell with dimensions of  $4a \times 4a \times 4a$  showed that the energies were almost the same as those obtained using the  $M_{108}H_1$  supercell with dimensions of  $3a \times 3a \times 3a$  (see Supplemental Material [36]). This indicates that chemical and/or elastic interactions between the H atoms under periodic boundary conditions are regarded as negligible when the distance between them is larger than approximately  $3a$  (i.e., 1.0–1.2 nm), which is ascribed to the fact that the H atom dissolved in the metal is essentially neutral and its atomic radius is very small.

### B. Jump rates and diffusivities of H

The path integral-based reaction free energy introduced by Gillan [8] corresponds to the reversible work of moving the center-of-mass positions (i.e., centroids) of ring polymers along the reaction coordinate [10,24,39–42]. Each of the obtained images along the MEP were assumed to correspond to the centroid configuration  $\mathbf{r}^{\text{cent}} = \{\mathbf{r}_I^{\text{cent}}\}$  ( $1 \leq I \leq N$ ) of the ring polymers in the  $N$ -particle system. For each individual centroid configuration, *ab initio* PIMD calculations were performed for 1000 steps with a time increment of 1 fs, using 32 and 12 beads for temperatures below and above 150 K, respectively (for details on *ab initio* PIMD calculations, see Supplemental Material [36]). Forces acting on the nuclei were calculated based on DFT using the PAW–PBE approximation with an  $E_{\text{cut}}$  of 250–300 eV and a  $6 \times 6 \times 6$   $k$ -point mesh. The path integral average of the centroid force  $\mathbf{f}^{\text{cent}}(\{\mathbf{r}_I^{(s)}\})$  was calculated for nine temperatures between 75 and 1200 K for a statistical ensemble of bead configurations  $\{\mathbf{r}_I^{(s)}\}$  with fixed centroid positions. The PIMD-based free-energy profiles were obtained via numerical integration of the centroid mean force along the H-migration pathway  $\mathbf{q}$  connecting states  $X$  and  $Y$ , i.e.,

$$\Delta F(\mathbf{q}_Y, \mathbf{q}_X) = - \int_{\mathbf{q}_X}^{\mathbf{q}_Y} d\mathbf{q} \cdot \frac{\langle \mathbf{f}^{\text{cent}}(\{\mathbf{r}_I^{(s)}\}) \delta(\mathbf{r}^{\text{cent}} - \mathbf{q}) \rangle_{\text{PI}}}{\langle \delta(\mathbf{r}^{\text{cent}} - \mathbf{q}) \rangle_{\text{PI}}}, \quad (1)$$

where  $\mathbf{q}_X$  and  $\mathbf{q}_Y$  represent the centroid configurations in which the H atom is located at either an O, T, or S site ( $X = \text{O or T}; Y = \text{S}$ ), and  $\delta$  is Dirac’s delta function. The bracket denotes the ensemble average of the quantity inside. The differences between the free energies of the system  $F_{Y-X}$  for H at different interstitial sites can be expressed as  $F_{S-O} \equiv \Delta F(\mathbf{q}_S, \mathbf{q}_O)$  and  $F_{S-T} \equiv \Delta F(\mathbf{q}_S, \mathbf{q}_T)$ .

Lattice diffusion of H in fcc metals, in which there are two T sites and one O site per metal atom, occurs via a series of jumps between the O and T sites, such that each  $\text{O} \rightarrow \text{T}$  jump must be followed by a  $\text{T} \rightarrow \text{O}$  jump. We assumed that the concentration of H in the metals is low, i.e., there are no interactions and blocking effects between the H atoms. In this case, all directions for jumps of an H atom to neighboring empty sites are equally probable and independent of the prior jump. Therefore, the jump sequence of the interstitial H atom under dilute conditions is uncorrelated [43]. The isotropic diffusivity

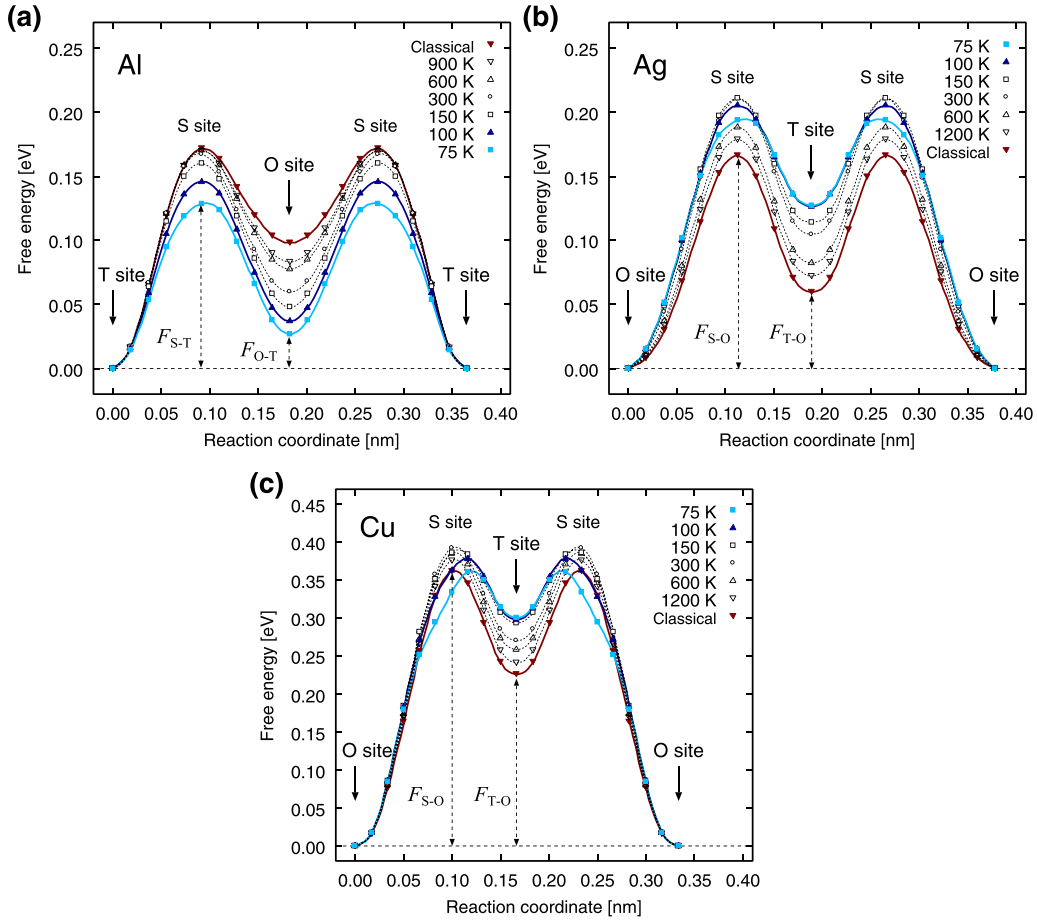


FIG. 1. Free-energy profiles for H migration in (a) Al, (b) Ag, and (c) Cu along T-O-T (or O-T-O) pathway at various temperatures.

for an O-T network in the fcc lattice without correlation is defined as [44]

$$D = \frac{a^2}{2} \rho_O \Gamma_{O \rightarrow T} = \frac{a^2}{2} \rho_T \Gamma_{T \rightarrow O}, \quad (2)$$

where  $\rho$  and  $\Gamma$  denote the equilibrium site probability and jump rate, respectively. The probabilities are expressed using these two rates as follows:

$$\rho_O = \frac{\Gamma_{T \rightarrow O}}{2\Gamma_{O \rightarrow T} + \Gamma_{T \rightarrow O}}, \quad \rho_T = \frac{\Gamma_{O \rightarrow T}}{2\Gamma_{O \rightarrow T} + \Gamma_{T \rightarrow O}}, \quad (3)$$

such that the normalization  $\rho_O + 2\rho_T = 1$  remains true. In this paper, we predicted the jump rates of H in fcc metals using  $F_{S-O}$ ,  $F_{S-T}$ , and a pre-exponential factor based on the one-dimensional probability distribution in a thermal ensemble [25,45]. The jump rate at which an H atom initially located around an O or T site ( $q_O$  or  $q_T$ ) escapes over the barrier is given as

$$\Gamma_{O \rightarrow T} = \frac{v^* \exp(-\beta F_{S-O})}{\int_O \exp[-\beta F_O(q)] dq},$$

$$\Gamma_{T \rightarrow O} = \frac{v^* \exp(-\beta F_{S-T})}{\int_T \exp[-\beta F_T(q)] dq}, \quad (4)$$

where  $dq$  represents a line element along the pathway, i.e.,  $dq = |dq|$ ;  $\beta$  is the inverse temperature  $(k_B T)^{-1}$ ;  $k_B$  is the Boltzmann constant; and  $T$  is the absolute temperature.  $F_O(q)$  and  $F_T(q)$  denote the one-dimensional free-energy profiles as

functions of  $q$ , where the zero energy is assumed to be at the bottom of the well corresponding to  $q_O$  and  $q_T$ , respectively. The integral in Eq. (4) runs between the two tops of the barriers (i.e., neighboring S sites) across the well.  $v^*$  is the forward flux at the top of the barrier, i.e.,  $(2\pi\beta m)^{-\frac{1}{2}}$ , with  $m$  being the mass of the diffusing particle.

Note that, in the present PIMD calculations, the considered metal-H systems maintained the fcc structure and did not melt even at temperatures above their melting points because the centroid positions of particles were fixed during the sampling of bead configurations (see Supplemental Material [36]). This indicates that the thermal fluctuation of particles is not explicitly included in the present model, while the temperature dependence of NQEs on phonon vibrations is, however, taken into account. In this paper, considering the experimental fact that the melting points of Al, Ag, and Cu are 933.5, 1234.9, and 1357.8 K, respectively [46], the results were analyzed for the temperature range of 75–900 K for Al and 75–1200 K for Ag and Cu. Caution must be practiced when referring to the PIMD results at temperatures close to melting points (e.g., at 900 K for Al, and 1200 K for Ag).

### III. RESULTS AND DISCUSSION

#### A. NQEs on H migration

Figure 1 shows the centroid-based free-energy profiles for H migration between T and O sites in Al, Ag, and Cu over the temperature range 75–1200 K (75–900 K for Al).

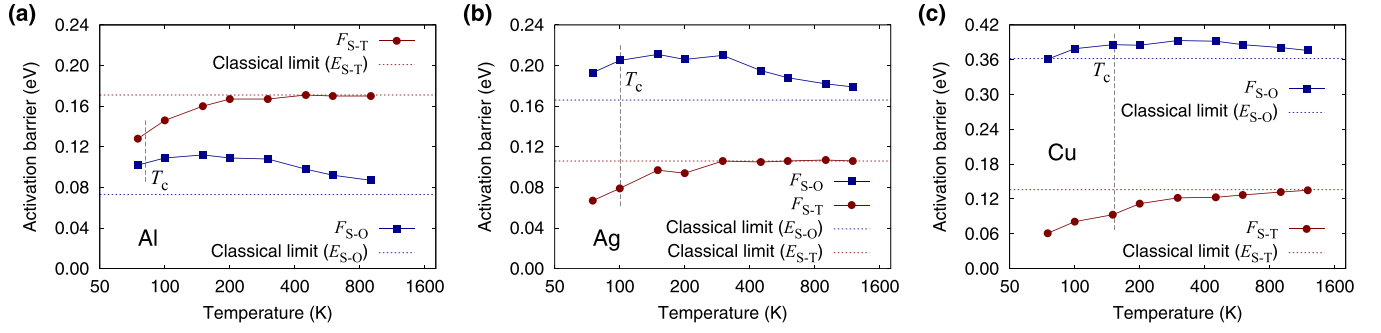


FIG. 2. Dependence of  $F_{S-O}$  and  $F_{S-T}$  of H on temperature, in (a) Al, (b) Ag, and (c) Cu. Vertical dotted lines represent crossover temperatures according to Eq. (5), i.e.,  $T_c = 81, 101,$  and  $153$  K for Al, Ag, and Cu, respectively.

Notice that H atoms in Al prefer T sites, whereas those in Ag and Cu prefer O sites. The H-migration barrier of Al (i.e.,  $F_{S-T}$  along the T–O–T pathway) changes monotonically as the temperature decreases; it changes only slightly above 200 K, whereas it decreases drastically at lower temperatures. On the other hand, the H-migration barriers of Ag and Cu (i.e.,  $F_{S-O}$  along the O–T–O pathway) behave differently: they increase in intermediate-temperature ranges and then decrease in low-temperature ranges. The  $F_{S-T}$  and  $F_{S-O}$  values of H in these metals are plotted as functions of temperature in Fig. 2. The  $F_{S-T}$  values are almost constant at high-to-intermediate temperatures and decrease at lower temperatures, whereas the  $F_{S-O}$  values increase, peak, and then decrease as the temperature decreases. The characteristic decrease in the H-migration barrier at low temperatures is ascribed to the onset of quantum tunneling, which is observed at temperatures within the ranges 150–200 K, 100–150 K, and 150–200 K for Al, Ag, and Cu, respectively, as shown in Fig. 2. The transition tends to occur quite abruptly below a certain crossover temperature, which is estimated as follows [9,47]:

$$T_c = \hbar\Omega_b/(2\pi k_B), \quad (5)$$

where  $\hbar$  represents the reduced Planck constant and  $\Omega_b$  is the angular frequency at the top of the barrier, i.e., the magnitude of the imaginary frequency corresponding to the reactive mode at the transition state.  $T_c$  denotes the temperature at which tunneling and thermally activated barrier crossing are of roughly equal importance. From the vibrational frequency analysis, we obtained  $\Omega_b = 8.3, 6.7,$  and  $12.5$  (in  $\times 10^{13}$  rad/s), such that  $T_c = 81, 101,$  and  $153$  K for Al, Ag, and Cu, respectively.

For these three metals, the  $F_{S-T}$  and  $F_{S-O}$  values approach their classical limits (i.e.,  $E_{S-T}$  and  $E_{S-O}$ , respectively) at high temperatures. Interestingly, NQEs are manifested even at rather high temperatures, as confirmed for H isotopes in fcc Pd [24,25]. A free-energy profile approaches its classical limit quite gradually with increasing temperature, such that the profile does not entirely reach the limit even at 1200 K. This implies that the quantum nature of H nuclei depending on temperature is crucial to understanding the precise kinetics of H migration in these fcc metals not only at low temperatures but also at high temperatures.

The site energies obtained from H-migration pathways were compared with those obtained from the previous DFT calculations [48,49]. In Fig. 2, the  $F_{O-T}$  ( $= F_{S-T} - F_{S-O}$ ) and

$F_{S-T}$  for H in Al at a temperature above 200 K are 0.06–0.09 and 0.17 eV, respectively, which agree well with the zero-point energy (ZPE)-corrected DFT values of 0.04 and 0.15 eV, respectively, reported by Wolverton *et al.* [48]. Moreover,  $F_{T-O}$  ( $= F_{S-O} - F_{S-T}$ ) for H in Cu at temperatures of 75–1200 K, which was obtained as 0.24–0.30 eV, is consistent with the ZPE-corrected DFT value of 0.23 eV reported by Zhou *et al.* [49]. The DFT results reported by Zhou *et al.* suggest that the barrier top along the H-migration pathway in Cu corresponds to a state where an interstitial H atom is located at the T site; therefore, the corresponding activation barrier was assumed equivalent to the difference between the solution energies of H at the O and T sites (i.e., the ZPE-corrected  $E_{T-O}$  of 0.23 eV). In contrast, our results clearly showed that the transition state for H migration actually lies between the stable O and metastable T sites. Thus, as shown in Fig. 1(c), the PIMD-based activation barrier for H migration along the O–T–O pathway (i.e.,  $F_{S-O}$  of 0.36–0.39 eV), which is compatible with experimental values of 0.36–0.42 eV [14,15,20], is obviously higher than  $F_{T-O}$ . To the best of our knowledge, no comparable DFT data have been reported for H diffusion in pure Ag.

## B. Quantum distribution and vibrational energy of H atom

To characterize the state of an H atom in an fcc metal, the quantum distributions of a ring polymer representing the H atom at three centroid positions for the O, T, and S sites were investigated. The size of the ring polymer was calculated based on the root-mean-square radius of gyration  $R_g$ , which is defined as

$$(R_g)^2 = \frac{1}{P} \left\langle \sum_{s=1}^P (r^{(s)} - r^{\text{cent}})^2 \right\rangle_{\text{PI}}, \quad (6)$$

where  $r^{\text{cent}}$  is the instantaneous one-dimensional centroid of the ring polymer. For a free particle with a mass of  $m$ , at the limit  $P \rightarrow \infty$  [9],

$$(R_g^{\text{fp}})^2 = \hbar^2/(12mk_B T) = \pi \Lambda^2/6, \quad (7)$$

where  $\Lambda$  is the thermal de Broglie wavelength. If the quantum particle is confined by a potential, then the low-temperature spreading is limited, and  $R_g$  approaches a constant as  $T \rightarrow 0$ . This can be examined analytically for a harmonic oscillator,

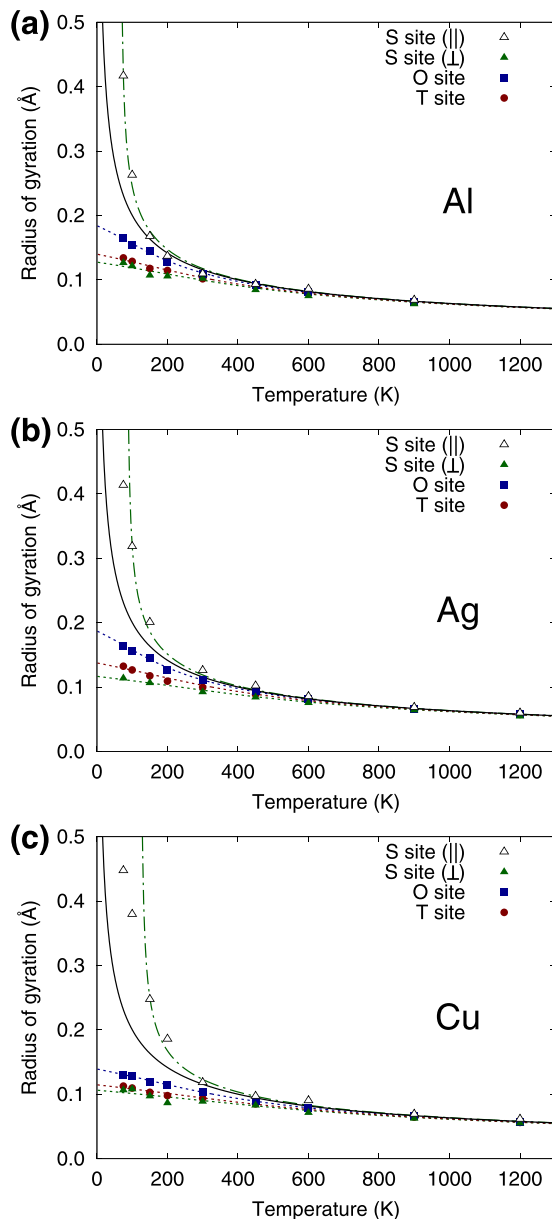


FIG. 3. Dependence of radius of gyration ( $R_g$ ) of the ring polymer representing H atom located at O, T, and S sites on temperature, in (a) Al, (b) Ag, and (c) Cu. Dotted and dashed-dotted curves represent fitting results based on Eq. (8) for real and imaginary frequencies, respectively, and  $\hbar\omega_0$  values obtained are listed in Table I. Solid curve represents the free-particle limit according to Eq. (7).

for which at the  $P \rightarrow \infty$  limit [9],

$$(R_g^{\text{ho}})^2 = \frac{k_B T}{m\omega_0^2} \left[ \frac{\hbar\omega_0}{2k_B T} \coth\left(\frac{\hbar\omega_0}{2k_B T}\right) - 1 \right], \quad (8)$$

where  $\omega_0$  is the oscillator's angular frequency.

We evaluated the three orthogonal components of the  $R_g$ 's of the quantum distributions of the H atom about the principal axes of inertia, as shown in Fig. 3. They are nearly degenerate at the O and T sites because of the cubic symmetry of the sites in the fcc lattice, whereas those at the S site exhibit a notable difference between the components parallel (||) and perpendicular ( $\perp$ ) to the H-migration pathway. At high

temperatures, the H-atom distributions at all sites are confined and almost isotropic, such that each distribution converges to the free-particle limit as the temperature increases. At low temperatures, on the other hand, the width of the distribution at each site varies. The distribution of H atoms at an O site is clearly confined but exhibits a relatively large spread because of the small curvature of the potential. Notably, the distribution at an S site parallel to an O–T pathway (i.e., corresponding to a reactive mode with an imaginary frequency) is significantly expanded beyond the free-particle limit, whereas those perpendicular to the pathway (i.e., corresponding to nonreactive modes with real frequencies) are much more localized than at a T site because of strong confinement. This indicates that such intersite migrations are significantly affected by the quantum delocalization of the H nucleus depending on temperature.

For the O, T, and S ( $\perp$ ) components, the effective vibrational energy  $\hbar\omega_0$ , which apparently includes anharmonic contributions to the vibrational frequency, was obtained via fitting of Eq. (8) to  $R_g$  as a function of  $\omega_0$ . In addition,  $\hbar\omega_0$  for the reactive mode [i.e., corresponding to the S (||) component] was obtained by the same fitting procedure based on Eq. (8) by replacing  $\omega_0$  by  $i\omega_0$ , where  $i$  represents the imaginary unit. The  $\hbar\omega_0$  values obtained are listed in Table I. For comparison, the vibrational frequencies  $\nu_j$  ( $1 \leq j \leq 3N - 3$ ) and energies  $h\nu_j$  (where  $h = 2\pi\hbar$ ) were calculated via harmonic vibrational analysis in such a way that the Hessian matrix of the system was determined from the forces acting on atoms within the classical DFT regime, in which each atom was displaced (by  $\pm 0.01\text{\AA}$ ) in the direction of each Cartesian coordinate. Among them, those of the H atom ( $\nu_j^{\text{H}}$  and  $h\nu_j^{\text{H}}$ , where  $j = 1, 2, 3$ ) are also listed in Table I. The degree of confinement of H atoms in Cu is clearly stronger than that in Al and Ag, because of the large curvature of the potential surface of H migration in Cu, as depicted in Fig. 1(c). Whereas H atoms in Al and Ag are confined to almost the same extent at the interstitial sites, the free-energy profiles for H migration in both metals exhibit qualitatively different behaviors with respect to temperature. We determined that anharmonic effects increase the vibrational energy of an H atom at an O site by 20 meV, whereas that at a T site is almost unchanged. This tendency is consistent with the DFT results reported by Wolverton *et al.* [48] for H in Al. Notably, the vibrational energies for the reactive mode estimated from the S (||) component of the  $R_g$ 's are consistently smaller than those obtained from the harmonic vibrational frequencies  $\Omega_b = 2\pi\nu_3^{\text{H}}$  (by 8–16 meV) at transition states for each metal, indicating that the anharmonicity of the potential seemingly reduces the curvature at the top of the barrier. These observations suggest that the anharmonic character of the potential-energy surface around the H-diffusion pathway, which is effectively incorporated in the *ab initio* PIMD calculations when delocalized states of the H atom are sampled, significantly influences the discrete vibrational energy levels of H.

### C. Jump rates

The PIMD-based jump rates of H atoms (i.e.,  $\Gamma_{\text{O} \rightarrow \text{T}}$  and  $\Gamma_{\text{T} \rightarrow \text{O}}$ ) in fcc Al, Ag, and Cu as functions of inverse temperature are shown in Fig. 4. The two jump rates exhibit

TABLE I. Vibrational energies of H atom located at O, T, and S sites in Al, Ag, and Cu obtained within classical DFT and PIMD regimes. The vibrational frequencies of the H atom at O and T sites are three-fold degenerate. The values in the parentheses are for the reactive mode with an imaginary frequency parallel to the migration pathway, while there are two degenerate modes with real frequencies perpendicular to the pathway at the S site. Symbol  $i$  represents imaginary unit.

System	Site	Classical DFT		PIMD
		Frequency, $\nu_j^H$ (THz)	$h\nu_j^H$ (meV)	$\hbar\omega_0$ (meV) [in Eq. (8)]
Al <sub>32</sub> H <sub>1</sub>	O	10.6, 10.6, 10.6	44	61
	T (stable)	24.9, 24.9, 24.9	103	106
	S	31.0, 31.0, (10.6 <i>i</i> )	128, (44)	127, (36)
Ag <sub>32</sub> H <sub>1</sub>	O (stable)	9.5, 9.5, 9.5	39	59
	T	26.1, 26.1, 26.1	108	110
	S	33.7, 33.7, (13.2 <i>i</i> )	140, (54)	152, (46)
Cu <sub>32</sub> H <sub>1</sub>	O (stable)	20.9, 20.9, 20.9	87	107
	T	36.2, 36.2, 36.2	150	158
	S	44.4, 44.4, (20.0 <i>i</i> )	183, (83)	183, (67)

differences in their dependence on temperature, namely, an inclined “reversed-S”-shaped curve for  $\Gamma_{O \rightarrow T}$  and a “C”-shaped curve for  $\Gamma_{T \rightarrow O}$ , on the Arrhenius plot. Similar trends have been reported for H-isotope diffusion in fcc Pd [25]. Figure 4 also shows the classical limits of the jump rates given by Eq. (4) when the NQEs are excluded. In the high-temperature region, both rates for each metal approach their classical limits, which are represented by almost straight lines in Fig. 4. As the temperature decreases,  $\Gamma_{O \rightarrow T}$  decreases in a concave-down fashion and deviates downward from linear behavior at the classical limit.  $\Gamma_{O \rightarrow T}$  then exhibits an inflection point at approximately  $T_c$ , and thereafter tends to decline

steadily in a concave-up fashion. In particular,  $\Gamma_{O \rightarrow T}$  for Cu eventually crosses over and exceeds its classical limit at approximately 75 K. Such a trend arises from the increase, peak, and then decrease in  $F_{S \rightarrow O}$  with decreasing temperature due to NQEs, as shown in Fig. 2.

From the temperature dependence of  $\Gamma_{O \rightarrow T}$ , shown schematically in Fig. 4(d), the temperature range considered in this paper is classified into three temperature regions such that each corresponds to a different diffusion regime: (i) a classical regime at high temperatures, (ii) a quantum-fluctuation-dominated regime at intermediate temperatures, and (iii) a quantum-tunneling-dominated regime at low

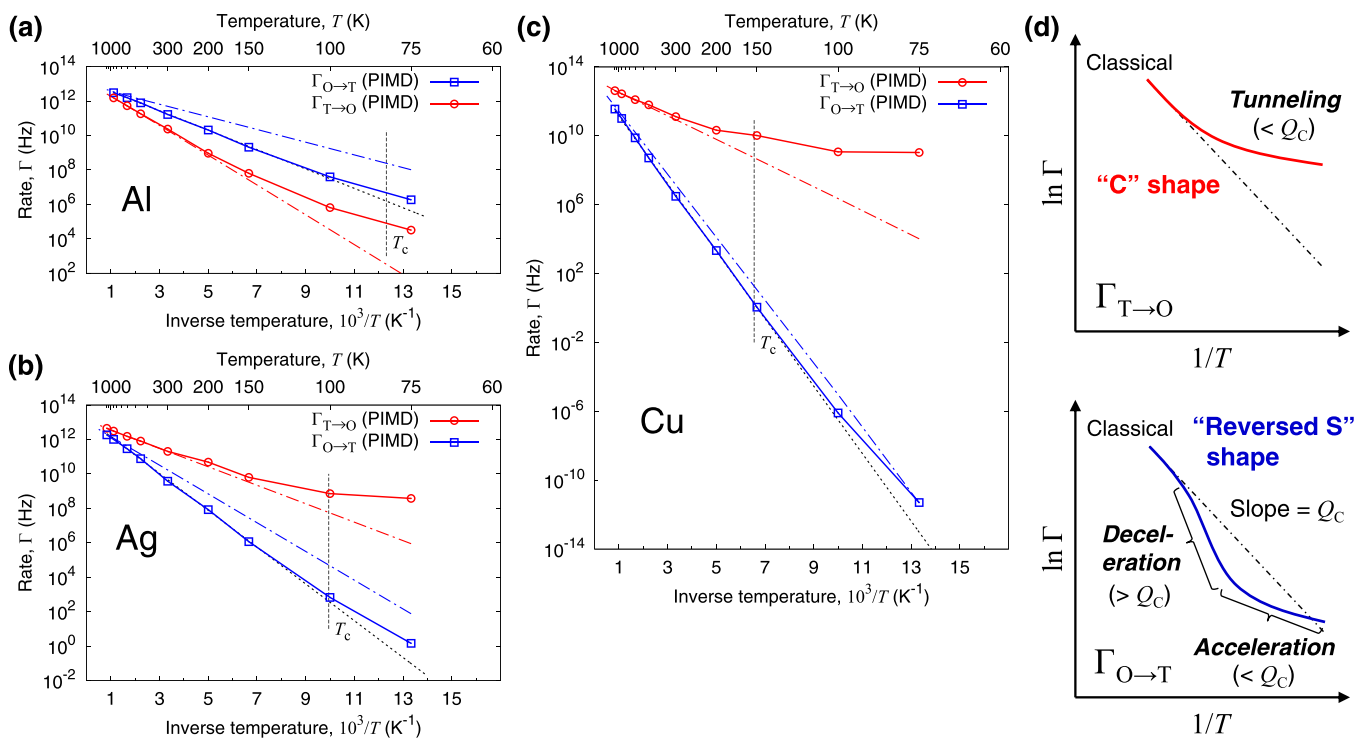


FIG. 4. Arrhenius plots of jump rates of H atom over the temperature range 75–1200 K (75–900 K for Al):  $\Gamma_{O \rightarrow T}$  (squares) and  $\Gamma_{T \rightarrow O}$  (circles) in (a) Al, (b) Ag, (c) Cu, and (d) their schematics. Dashed-dotted curves represent classical limits. Dotted line represents Arrhenius fit of  $\Gamma_{O \rightarrow T}$  in the intermediate-temperature range 200–600 K. Vertical dotted lines represent crossover temperatures according to Eq. (5), i.e.,  $T_c = 81, 101,$  and  $153$  K for Al, Ag, and Cu, respectively.

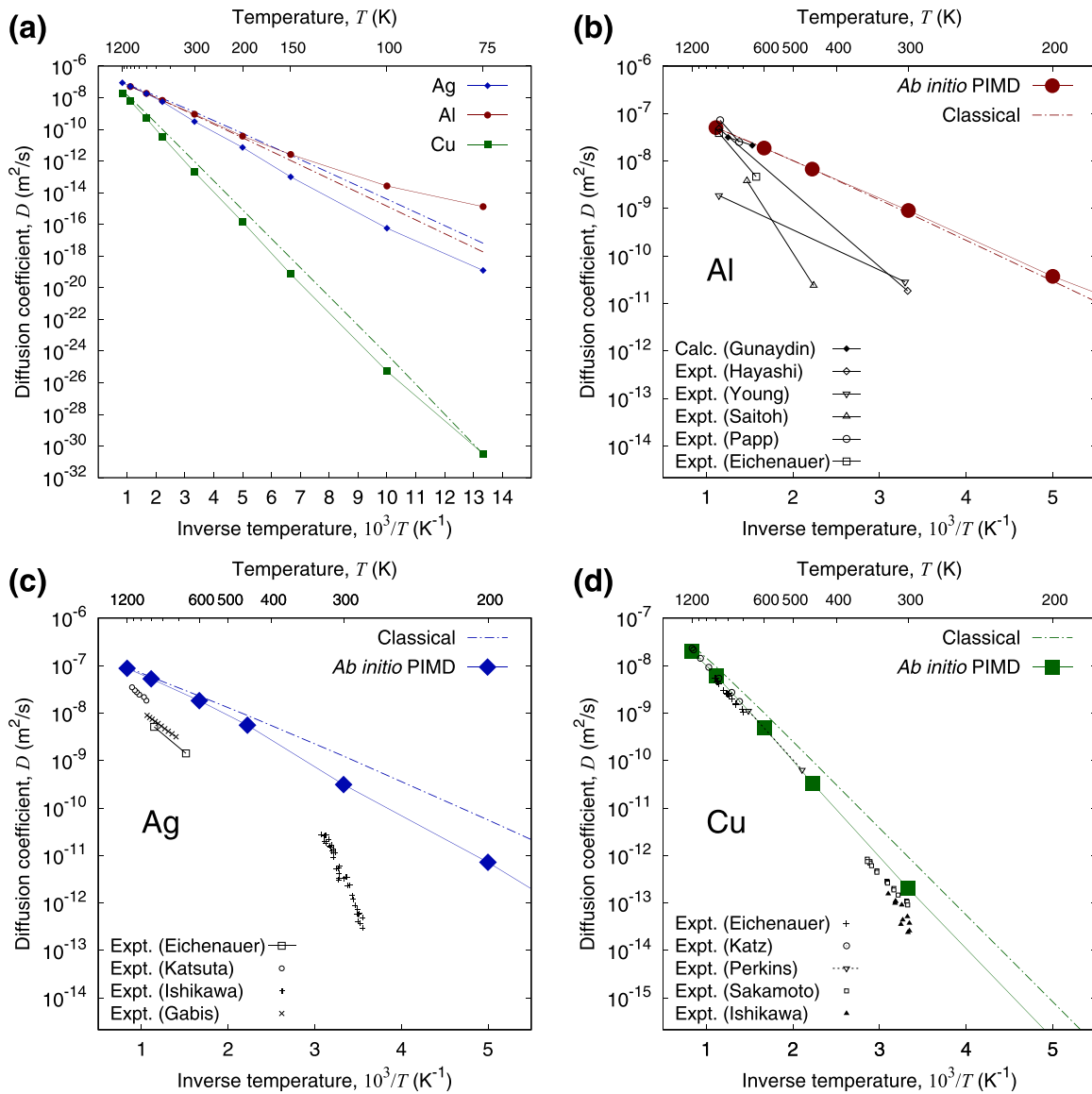


FIG. 5. Diffusion coefficients of H in Al, Ag, and Cu, as functions of inverse temperature: (a) results for the temperature range 75–1200 K and enlarged views in range 200–1200 K for (b) Al, (c) Ag, and (d) Cu. Note that the upper temperature is limited to 900 K for Al so as not to exceed its melting point. Solids plots represent *ab initio* PIMD results, where dependence on temperature for Ag and Cu exhibits reversed-S shapes, whereas that for Al exhibits C shape. Dashed-dotted curves represent classical limits. Experimental data were obtained from Refs. [50–54,63] for Al, Refs. [55–58] for Ag, and Refs. [14,15,59–61] for Cu.

temperatures. Here, we use the term “quantum fluctuation” to refer to the motion of quantum particles mainly due to zero-point vibrations and quantization of energy levels among various NQEs. With reference to the high-temperature classical limit  $Q_c$  of the slope of the Arrhenius plot, the intermediate-temperature region after the transition from (i) to (ii) has a slope higher than  $Q_c$ , indicating the regime in which the H diffusion is inhibited by an elevated barrier due to quantum fluctuations. By contrast, the low-temperature region after the transition from (ii) to (iii) has a slope lower than  $Q_c$ , indicating the regime in which the H diffusion is assisted by a reduced barrier due to quantum tunneling. Of the three vibrational modes of the H atom, one parallel to the pathway [i.e.,  $S(\parallel)$ ] is responsible for the quantum tunneling at low

temperatures, whereas the other two perpendicular to the H-migration pathway [i.e.,  $S(\perp)$ ] are supposed to be responsible for the quantum fluctuations at intermediate temperatures, as suggested in Fig. 3. In Fig. 4, the  $T_c$  estimated from the barrier frequency is rather compatible with the onset temperature of the transition from (ii) to (iii) in each metal.

On the other hand, the dependence of  $\Gamma_{T \rightarrow O}$  on temperature exhibits a familiar “C”-shaped curve in the Arrhenius plots;  $\Gamma_{T \rightarrow O}$  deviates upward from the classical limit and tends to level off at 150–300 K, which is much higher than the estimated  $T_c$ . An upturn in the rate indicates the onset of quantum tunneling associated with a transition from (i) to (iii), skipping the region of (ii). This suggests that the effect of quantum fluctuations is smaller than that of quantum

tunneling for  $\Gamma_{T \rightarrow O}$ , compared with that for  $\Gamma_{O \rightarrow T}$ , such that deceleration of the H jump becomes difficult to occur in the intermediate-temperature range.

As temperature decreases, the difference between  $\Gamma_{O \rightarrow T}$  and  $\Gamma_{T \rightarrow O}$  for Ag and Cu increases more drastically, as shown in Figs. 4(b) and 4(c). By contrast, for Al, the difference remains within a certain range even at low temperatures, as observed in Fig. 4(a). This indicates that H diffusions in Ag and Cu, which are dominated by  $\Gamma_{O \rightarrow T}$ , are impeded by NQEs over a wide range of temperatures. By contrast, that in Al, which is dominated by  $\Gamma_{T \rightarrow O}$ , is assisted by the NQEs.

#### D. H diffusivities

According to Eqs. (2) and (3), the diffusion coefficients ( $D$ ) of interstitial H in fcc Al, Ag, and Cu were predicted from the PIMD values of  $\Gamma_{O \rightarrow T}$  and  $\Gamma_{T \rightarrow O}$ . This is the first case of predicting H diffusivities in these metals while considering the temperature-dependent NQEs in an *ab initio* manner. Figure 5(a) shows the Arrhenius plots of  $D$  for H in Al, Ag, and Cu in the temperature range of 75–1200 K (75–900 K for Al). For reference, the corresponding  $D$  values are listed in Table S2 (within the Supplemental Material [36]). In the PIMD results, the logarithmic value of  $D$  changes nonlinearly with the inverse temperature, such that the curve is C-shaped for Al, and reversed-S-shaped for Ag and Cu because of the characteristic change in  $F_{S,O}$  and  $F_{S,T}$  with respect to temperature, as shown in Fig. 2.

In Fig. 5(a), the  $D$  values of H in Ag are among the highest for the three metals above 900 K. Similar to the reversed-S-shaped dependence of  $\Gamma_{O \rightarrow T}$  on temperature, the  $D$  values in Ag and Cu, as the temperature decreases, decline in a concave-down fashion and deviate downward from linear behavior at the classical limit. Afterward, at low temperatures,  $D$  exhibits an inflection point and tends to decrease steadily in a concave-up fashion. On the other hand, similar to the C-shaped dependence of  $\Gamma_{T \rightarrow O}$  on temperature, the  $D$  values in Al, as the temperature decreases, deviate upward from the classical limit and exceed those in Ag at approximately 600 K.

For comparison, the experimental  $D$  values for Al [50–54], Ag [55–58], and Cu [14,15,59–61] are plotted in Figs. 5(b)–5(d). The experimental  $D$  values for Cu are observed to be consistent with each other in the temperature range 300–1198 K, whereas large variations exist in those for Al and Ag. In Figs. 5(b)–5(d), the PIMD results for Cu agree well with experimental measurements over a wide range of temperatures, whereas those for Al and Ag differ from the experimental values except in the high-temperature region. However, our  $Q$  value for Al agrees well with recent experimental  $Q$  measurements of 0.17–0.18 eV [54,62]. Furthermore, the  $D$  values reported by Gunaydin *et al.* [63], which were obtained using the Born-Oppenheimer molecular dynamics method at high

temperatures, are consistent with our results. In the case of Al, the PIMD results show that  $D$  as a function of inverse temperature can be linearly approximated in the temperature range above 200 K, below which, however, it deviates from linear dependence because of the onset of tunneling. Interestingly, the PIMD-based  $D$  values for Ag significantly deviate downward from those for Al over a wide temperature range of 150–900 K, whereas the classical limits of the H-migration barriers for Al and Ag are almost the same, such that, in the temperature range examined in this study,  $Q_c$  for Al (i.e.,  $E_{S,T}$  of 0.171 eV) corresponds to the upper limit of  $Q$  and that for Ag (i.e.,  $E_{S,O}$  of 0.166 eV) to the lower limit of  $Q$ . Such an irregular evolution is attributable to the two distinct temperature-dependent jump rates in the Arrhenius plots, as shown in Fig. 4, arising from differences in the temperature dependence of the NQEs and the different site preferences of interstitial H atoms in the host metals.

#### IV. CONCLUSIONS

Using *ab initio* PIMD, we elucidated a comprehensive microscopic picture of the temperature-dependent diffusivities of H in common fcc metals such as Al, Ag, and Cu, which has not yet been either experimentally or theoretically clarified. Interestingly, the Arrhenius plots of H diffusivities in Ag and Cu had a reversed-S-shaped curve, which is consistent with that reported for H in Pd, whereas that in Al had a C-shaped curve. The results indicate that two distinct temperature-dependent jump rates of H coexist in each metal and determine whether the H diffusion is impeded or assisted by NQEs, depending on the preferential H location at the interstitial sites with different curvatures of the potential. This was determined through our computational approach, which can extract the rate-determining step in the diffusion of H in metals, allowing us to examine whether the H diffusion is governed by reversed-S-type  $\Gamma_{O \rightarrow T}$  or C-type  $\Gamma_{T \rightarrow O}$ . Such a mechanism is considered to be common in other fcc metals with similar dependence on temperature of the free-energy barrier for H migration. We expect that our findings will serve as a basis for the development of novel strategies to enhance or inhibit H diffusion in materials through control of NQEs by tuning potential-energy surfaces for systems.

#### ACKNOWLEDGMENTS

This work was supported by Grants-in-Aid for Scientific Research (B) (Grants No. 21H01603 and No. 18H01693) from the Japan Society for the Promotion of Science (JSPS). M.S. acknowledges the support by Grant-in-Aid for Scientific Research on Innovative Areas (Grant No. 18H05519) from the Ministry of Education, Culture, Sports, Science and Technology (MEXT) of Japan and by the JAEA supercomputer facility.

- [1] Y. Fukai, *The Metal-Hydrogen System: Basic Bulk Properties*, 2nd ed. (Springer, Berlin, 2005).  
 [2] J. J. Conde, M. Maroño, and J. M. Sánchez-Hervás, *Sep. Purif. Rev.* **46**, 152 (2017).

- [3] R. Mohtadi and S. Orimo, *Nat. Rev. Mater.* **2**, 16091 (2017).  
 [4] L. Schlappbach and A. Züttel, *Nature (London)* **414**, 353 (2001).  
 [5] R. A. Causey, *J. Nucl. Mater.* **300**, 91 (2002).

- [6] J. Völkl and G. Alefeld, in *Hydrogen in Metals I: Basic Properties*, Topics in Applied Physics Vol. 28, edited by G. Alefeld and J. Völkl (Springer, Berlin, 1978), pp. 321–348.
- [7] H. Wipf, in *Hydrogen in Metals III: Properties and Applications*, Topics in Applied Physics Vol. 73, edited by H. Wipf (Springer, Berlin, 1997), pp. 51–91.
- [8] M. J. Gillan, *Phys. Rev. Lett.* **58**, 563 (1987).
- [9] M. J. Gillan, *Philos. Mag. A* **58**, 257 (1988).
- [10] H. Kimizuka, H. Mori, and S. Ogata, *Phys. Rev. B* **83**, 094110 (2011).
- [11] T. Yoshikawa, T. Takayanagi, H. Kimizuka, and M. Shiga, *J. Phys. Chem. C* **116**, 23113 (2012).
- [12] I. H. Katzarov, D. L. Pashov, and A. T. Paxton, *Phys. Rev. B* **88**, 054107 (2013).
- [13] D. Di Stefano, M. Mrovec, and C. Elsässer, *Phys. Rev. B* **92**, 224301 (2015).
- [14] W. Eichenauer, W. Löser, and H. Witte, *Z. Metallkd.* **56**, 287 (1965).
- [15] L. Katz, M. Guinan, and R. J. Borg, *Phys. Rev. B* **4**, 330 (1971).
- [16] J. Völkl, G. Wollenweber, K.-H. Klatt, and G. Alefeld, *Z. Naturforsch. A* **26**, 922 (1971).
- [17] K. Yamakawa, *J. Phys. Soc. Jpn.* **47**, 114 (1979).
- [18] G. Sicking, *J. Less-Common Met.* **101**, 169 (1984).
- [19] G. Higelin, H. Kronmüller, and R. Lässer, *Phys. Rev. Lett.* **53**, 2117 (1984).
- [20] K. Yamakawa, K. Nunogaki, and F. E. Fujita, *J. Phys. Soc. Jpn.* **55**, 877 (1986).
- [21] G. L. Powell and J. R. Kirkpatrick, *Phys. Rev. B* **43**, 6968 (1991).
- [22] T. E. Markland and M. Ceriotti, *Nat. Rev. Chem.* **2**, 0109 (2018).
- [23] M. Ceriotti, W. Fang, P. G. Kusalik, R. H. McKenzie, A. Michaelides, M. A. Morales, and T. E. Markland, *Chem. Rev.* **116**, 7529 (2016).
- [24] H. Kimizuka, S. Ogata, and M. Shiga, *Phys. Rev. B* **97**, 014102 (2018).
- [25] H. Kimizuka, S. Ogata, and M. Shiga, *Phys. Rev. B* **100**, 024104 (2019).
- [26] J. R. Scully, G. A. Young, Jr., and S. W. Smith, in *Gaseous Hydrogen Embrittlement of Materials in Energy Technologies*, edited by R. P. Gangloff and B. P. Somerday (Woodhead, Cambridge, 2012), Vol. 2, pp. 707–768.
- [27] R. A. Causey, R. A. Karnesky, and C. S. Marchi, in *Comprehensive Nuclear Materials*, edited by R. J. M. Konings (Elsevier, Amsterdam, 2012), Vol. 4, pp. 511–549.
- [28] M. Li and S. J. Zinkle, in *Comprehensive Nuclear Materials*, edited by R. J. M. Konings (Elsevier, Amsterdam, 2012), Vol. 4, pp. 667–690.
- [29] G. Kresse and J. Furthmüller, *Phys. Rev. B* **54**, 11169 (1996).
- [30] P. E. Blöchl, *Phys. Rev. B* **50**, 17953 (1994).
- [31] G. Kresse and D. Joubert, *Phys. Rev. B* **59**, 1758 (1999).
- [32] J. P. Perdew, K. Burke, and M. Ernzerhof, *Phys. Rev. Lett.* **77**, 3865 (1996).
- [33] H. J. Monkhorst and J. D. Pack, *Phys. Rev. B* **13**, 5188 (1976).
- [34] M. Methfessel and A. T. Paxton, *Phys. Rev. B* **40**, 3616 (1989).
- [35] H. Jónsson, G. Mills, and K. W. Jacobsen, in *Classical and Quantum Dynamics in Condensed Phase Simulations*, edited by B. J. Berne, G. Ciccotti, and D. F. Coker (World Scientific, Singapore, 1998), Chap. 16, pp. 385–404.
- [36] See Supplemental Material at <http://link.aps.org/supplemental/10.1103/PhysRevMaterials.5.065406> for additional information on the numerical methods and extended data, which includes Refs. [64–69].
- [37] D. Marx and M. Parrinello, *J. Chem. Phys.* **104**, 4077 (1996).
- [38] M. Shiga, M. Tachikawa, and S. Miura, *J. Chem. Phys.* **115**, 9149 (2001).
- [39] G. Mills and H. Jónsson, *Phys. Rev. Lett.* **72**, 1124 (1994).
- [40] M. E. Tuckerman and D. Marx, *Phys. Rev. Lett.* **86**, 4946 (2001).
- [41] H. Kimizuka and S. Ogata, *Phys. Rev. B* **84**, 024116 (2011).
- [42] M. Shiga and H. Fujisaki, *J. Chem. Phys.* **136**, 184103 (2012).
- [43] H. Mehrer, *Diffusion in Solids: Fundamentals, Methods, Materials, Diffusion-Controlled Processes* (Springer, Berlin, 2007), Chap. 7.
- [44] D. R. Trinkle, *Philos. Mag.* **96**, 2714 (2016).
- [45] D. Chandler, *J. Chem. Phys.* **68**, 2959 (1978).
- [46] G. W. C. Kaye and T. H. Laby, *Tables of Physical and Chemical Constants*, 16th ed. (Longman, Essex, 1995), Sec. 3.10.
- [47] V. I. Goldanskii, *Dokl. Akad. Nauk SSSR* **124**, 1261 (1959).
- [48] C. Wolverton, V. Ozoliņš, and M. Asta, *Phys. Rev. B* **69**, 144109 (2004).
- [49] H.-B. Zhou, Y. Zhang, and X. Ou, *Comput. Mater. Sci.* **79**, 923 (2013).
- [50] W. Eichenauer, K. Hattenbach, and A. Pebler, *Z. Metallkd.* **52**, 682 (1961).
- [51] K. Papp and E. Kovács-Csetényi, *Scr. Metall.* **15**, 161 (1981).
- [52] H. Saitoh, Y. Iijima, and H. Tanaka, *Acta Metall. Mater.* **42**, 2493 (1994).
- [53] S. Hayashi, *Jpn. J. Appl. Phys.* **37**, 930 (1998).
- [54] G. A. Young, Jr. and J. R. Scully, *Acta Mater.* **46**, 6337 (1998).
- [55] W. Eichenauer, H. Künzig, and A. Pebler, *Z. Metallkd.* **49**, 220 (1958).
- [56] H. Katsuta and R. B. McLellan, *Scr. Metall.* **13**, 65 (1979).
- [57] T. Ishikawa and R. B. McLellan, *Acta Metall.* **33**, 1979 (1985).
- [58] I. Gabis, A. A. Kurdyumov, S. N. Mazayev, T. A. Ovsyannikova, and N. I. Timofeyev, *Phys. Met. Metallogr.* **69**, 90 (1990).
- [59] W. G. Perkins and D. R. Begeal, *Ber. Bunsenges. Phys. Chem.* **76**, 863 (1972).
- [60] Y. Sakamoto and K. Takao, *J. Japan Inst. Metals* **46**, 285 (1982).
- [61] T. Ishikawa and R. B. McLellan, *J. Phys. Chem. Solids* **46**, 445 (1985).
- [62] J.-H. Ai and J. R. Scully, *Corrosion* **69**, 752 (2013).
- [63] H. Gunaydin, S. V. Barabash, K. N. Houk, and V. Ozoliņš, *Phys. Rev. Lett.* **101**, 075901 (2008).
- [64] M. E. Tuckerman, B. J. Berne, G. J. Martyna, and M. L. Klein, *J. Chem. Phys.* **99**, 2796 (1993).
- [65] J. Cao and G. J. Martyna, *J. Chem. Phys.* **104**, 2028 (1996).
- [66] S. Nosé, *J. Chem. Phys.* **81**, 511 (1984).
- [67] W. G. Hoover, *Phys. Rev. A* **34**, 2499 (1986).
- [68] D. J. Tobias, G. J. Martyna, and M. L. Klein, *J. Phys. Chem.* **97**, 12959 (1993).
- [69] G. J. Martyna, M. E. Tuckerman, D. J. Tobias, and M. L. Klein, *Mol. Phys.* **87**, 1117 (1996).